ICAS 2016
30th Congress of the International Council of the Aeronautical Sciences
DCC, Daejeon, Korea ; September 25-30, 2016

PRECISION LANDING BASED ON ATMOSPHERIC DISTURBANCE MONITORING AND MODEL PREDICTIVE CONTROL

Norbert Siepenkötter*, Dieter Moormann*
*** Institute of Flight System Dynamics, RWTH Aachen University, Germany**

Keywords: *Precision Landing, Model Predictive Control*

Abstract

This paper presents an analysis of the applicability of atmospheric disturbance monitoring ahead of an aircraft to support high precision automatic landing. A model predictive control scheme is implemented that uses a linear model of the lateral motion of the aircraft as well as wind data measured ahead of the aircraft to minimize the wind induced deviations from the desired flight track.

A series of simulations is performed to assess control behavior, in particular with respect to limitations of the wind data availability. Special emphasis is put on the influence of the sensor range of a forward looking wind sensor.

The simulation results show that the controller is suitable for this task and that the incorporation of atmospheric disturbance measurements into the control scheme is able to enhance control performance significantly.

1 Introduction

Recent research in the application of Doppler Light Detection And Ranging (Doppler LIDAR) for wake vortex and wind shear detection [1], low level turbulence detection at airports [2][3][4] and in flight turbulence detection [5] indicates an availability of systems in the near future, that will allow a precise measurement of spatial atmospheric conditions in front of an aircraft.

Since atmospheric disturbances are by far the biggest contributors to deviation in touch-down position during landing [6], in this paper a method is developed and analyzed that counteracts the effects of those disturbances based on wind data measurements in front of the aircraft.

Current autoland systems are designed to give lateral touch-down accuracy in the range of several meters, even under adverse atmospheric conditions (Fig.1). This is generally sufficient to land on typically 40-60 m wide runways.

Feasibility studies on the operation of gear-less aircraft, capable to take-off and land (TOL) on a ground-based acceleration/deceleration vehicle (Fig.2) [7][8][9], however showed a strong requirement for automatic landing systems that offer a significantly better landing accuracy, compared to those currently available.

Such future concepts require a lateral touch-down accuracy of less than 1 m due to the necessity to synchronize lateral position and velocity of the aircraft with a ground-based vehicle (e.g. sledge) for rendezvous and landing. The relative longitudinal touch-down accuracy has to be in the same magnitude, but given its

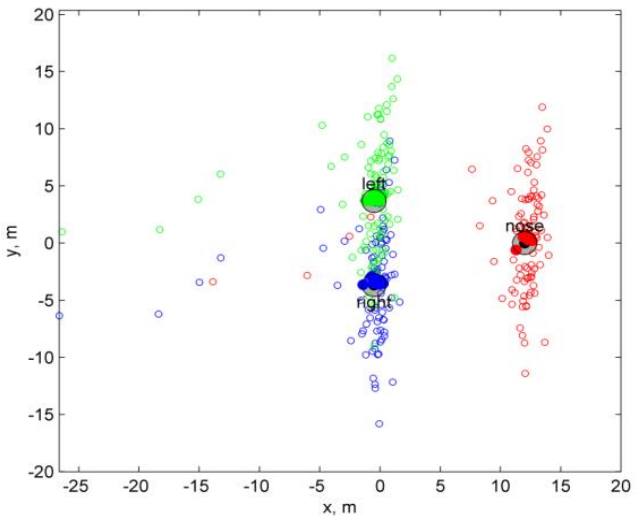

Fig. 1: Typical landing gear positions at Touch-down (*V*wind = 25 kts, von Karman turbulence, moving ground vehicle) [7]

Fig. 2: Gear-less aircraft on acceleration/ deceleration vehicle [8]

more agile longitudinal dynamic characteristics, it is more likely that the ground vehicle will be responsible here. Landing accuracy was identified as one of the key factors to enable the concept of gear-less aircraft [8].

Besides that, even for conventional runways an increase in lateral touch-down accuracy can improve landing safety and could ultimately lead to narrower and thus more cost effective runways.

1.1 Doppler LIDAR

Doppler LIDAR [1][3] uses a laser transceiver to emit a single-frequency pulsed laser light into the air and to receive light backscattered by aerosol particles in order to observe the motion of distant airflow. The frequency shift (Doppler Effect) of the backscattered light caused by the motion of the aerosols is used to determine the component of the wind speed along the optical axis while the round-trip time of the light is used to determine the distance of the observation.

Coplanar combination of two rotating LIDAR transceivers in their plane of operation allows the measurement of a 2-dimensional velocity distribution in this plane.

1.2 Model predictive control

Model Predictive Control (MPC) [10], also referred to as Moving Horizon Optimal Control or Receding Horizon Control, is a control method that is based on a discrete-time dynamic model that is used to estimate future reaction of the system with respect to the system's input variables. A cost function that can include objectives for input and output variables as well as system restrictions is iteratively minimized for a finite time horizon (prediction horizon) and control is achieved by applying the resulting control inputs to the controlled system for the current time slot. The prediction horizon is then successively shifted forward through time. MPC has thus the inherent ability to account for anticipated future events (e.g. gusts on the flight path) and to initiate control actions accordingly.

Originally developed for process control in chemical plants, MPC has already been introduced into many other fields of application, including experimental control of aircraft.

2 Control method using measured wind data

LIDAR measurements of the motion of the air mass between an approaching aircraft and the runway (or ground vehicle) can either be done on ground or on-board the aircraft. The measured velocities are then incorporated into a MPC feed forward control concept for the autoland controller to counteract the atmosphere-induced aircraft motion and resulting deviations in landing position.

In the MPC algorithm a linear model is used for the internal representation of the aircraft dynamics, due to the convenience of efficient numerical handling. The use of the linear model is justified, when nonlinearities are small in the vicinity of the point of linearization and the deviation from that point is also small.

The control performance of the MPC algorithm is evaluated by a set of monte-carlo simulations, taking into account the stochastic characteristics of atmospheric disturbances. The numerical analysis was performed using the *Model Predictive Control Toolbox* with *MATLAB/Simulink*.

The following chapters will explain the chosen models for the aircraft, wind and wind sensor and present simulation results for different sensor configurations.

2.1 Linear aircraft model

The rigid body motion of an aircraft can be formulated as two nonlinear vector differential

equations, one for the translational ($\vec{V}_\mathrm{K}$) and one for the angular velocities ($\vec{\Omega}_\mathrm{K}$) [11]:

$$\left(\frac{\mathrm{d}\vec{V_\mathrm{K}}}{\mathrm{d}t}\right)_b = \frac{1}{m}\underline{M}_{ba}\begin{bmatrix}X^\mathrm{A}\\Y^\mathrm{A}\\Z^\mathrm{A}\end{bmatrix}_a + \frac{1}{m}\begin{bmatrix}X^\mathrm{T}\\Y^\mathrm{T}\\Z^\mathrm{T}\end{bmatrix}_b + \begin{bmatrix}-\sin\Theta\\\sin\Phi\cos\Theta\\\cos\Phi\cos\Theta\end{bmatrix}g - \begin{bmatrix}q_\mathrm{K}w_\mathrm{K} - r_\mathrm{K}v_\mathrm{K}\\r_\mathrm{K}u_\mathrm{K} - p_\mathrm{K}w_\mathrm{K}\\p_\mathrm{K}v_\mathrm{K} - q_\mathrm{K}u_\mathrm{K}\end{bmatrix}_b \quad (1)$$

$$\left(\frac{\mathrm{d}\vec{\Omega_\mathrm{K}}}{\mathrm{d}t}\right) = \underline{T_b}^{-1}\left(\begin{bmatrix}L^\mathrm{A}+L^\mathrm{F}\\M^\mathrm{A}+M^\mathrm{F}\\N^\mathrm{A}+N^\mathrm{F}\end{bmatrix} - \frac{1}{m}\begin{bmatrix}q_\mathrm{K}r_\mathrm{K}(I_z-I_y) - p_\mathrm{K}q_\mathrm{K}I_{xz}\\r_\mathrm{K}p_\mathrm{K}(I_x-I_z) - (p_\mathrm{K}{}^2 - r_\mathrm{K}{}^2)I_{xz}\\p_\mathrm{K}q_\mathrm{K}(I_y-I_x) - p_\mathrm{K}r_\mathrm{K}I_{xz}\end{bmatrix}\right) \quad (2)$$

Here, $\underline{M}_{ba}$ denotes the transformation matrix between body-fixed (subscript *b*) and aerodynamic (subscript *a*) axis system, u_K, v_K, w_K, p_K, q_K, r_K the translational and angular velocities, X, Y, Z, L, M, N the aerodynamic (superscript A) and thrust (superscript T) forces and moments, Θ and Φ the pitch and roll angle and m, $\underline{T_b}$, I, and g the mass, inertia tensor, inertial tensor coefficients and gravitational constant.

In order to linearize equations (1) and (2), they will be simplified first by neglecting small contributions [11]. The angular velocities p_K, q_K and r_K are considered to be small, and thus the Euler term in (2) is eliminated. Furthermore, if the velocities orthogonal to the direction of flight (v_K and w_K) are small, the Euler term in (1) can be simplified to $[0 \;\; r_\mathrm{K}V_\mathrm{K} \;\; -q_\mathrm{K}V_\mathrm{K}]^\mathrm{T}$ with $V_\mathrm{K} \approx u_\mathrm{K}$. Additionally, for small angles α, β, Θ and Φ, the trigonometric functions of the flow angles can be replaced by a first order Taylor approximation. With the aerodynamic lift F_L, drag F_D, side force F_Y and the thrust line angle i_F, equations (1) and (2) become:

$$\begin{bmatrix}\dot{u}_\mathrm{K}\\\dot{v}_\mathrm{K}\\\dot{w}_\mathrm{K}\end{bmatrix}_b = \frac{1}{m}\begin{bmatrix}-F_\mathrm{D}+\alpha F_\mathrm{L}+F\\F_\mathrm{Y}\\-\alpha F_\mathrm{D}-F_\mathrm{L}-i_\mathrm{F}F\end{bmatrix}_e + \begin{bmatrix}-\sin\Theta\\\sin\Phi\cos\Theta\\\cos\Phi\cos\Theta\end{bmatrix}g + \begin{bmatrix}0\\-r_\mathrm{K}V_\mathrm{K}\\q_\mathrm{K}V_\mathrm{K}\end{bmatrix}_b \quad (3)$$

$$\begin{bmatrix}\dot{p}_\mathrm{K}\\\dot{q}_\mathrm{K}\\\dot{r}_\mathrm{K}\end{bmatrix}_b = \begin{bmatrix}\frac{I_z}{\Delta} & 0 & \frac{I_{zx}}{\Delta}\\0 & \frac{1}{I_y} & 0\\\frac{I_{zx}}{\Delta} & 0 & \frac{I_x}{\Delta}\end{bmatrix}_b \begin{bmatrix}L^\mathrm{A}\\M^\mathrm{A}\\N^\mathrm{A}\end{bmatrix}, \text{with } \Delta = I_xI_z - I_{zx}^2 \quad (4)$$

Landing accuracy is measured by the difference between actual and desired position of touch down. Therefore, the differential equation of the position needs to be added to the aircraft model. It can be expressed conveniently by defining a reference flight path (e.g. along a localizer) with flight-path azimuth $\chi_\mathrm{ref} = 0°$ and angle of climb $\gamma_\mathrm{ref} = 0°$. Then, with $\overrightarrow{\Delta R}$ as deviation from the reference flight path, the differential equation for the position becomes:

$$\dot{\overrightarrow{\Delta R}} = \begin{bmatrix}\Delta\dot{R}_x\\\Delta\dot{R}_y\\\Delta\dot{R}_z\end{bmatrix}_b = \begin{bmatrix}-\Delta V_\mathrm{K}\\-\Delta\chi V_\mathrm{K}\\\Delta\gamma V_\mathrm{K}\end{bmatrix} \quad (5)$$

Finally, to complete the aircraft model, the wind differential equation has to be added to the set of equations. For an aircraft that is flying in a wind field, the wind velocities it is affected by depend on the motion of the wind and on the motion of the aircraft itself. With Taylor's hypothesis of a "frozen" atmosphere and the outer product $\otimes$, the time derivative of the wind velocities can be simplified as:

$$\begin{bmatrix}\dot{u}_\mathrm{W}\\\dot{v}_\mathrm{W}\\\dot{w}_\mathrm{W}\end{bmatrix} = \left(\vec{\nabla}\otimes\vec{V}_\mathrm{W}\right)^T\vec{V}_\mathrm{K} = \begin{bmatrix}u_{\mathrm{W}x} & u_{\mathrm{W}y} & u_{\mathrm{W}z}\\v_{\mathrm{W}x} & v_{\mathrm{W}y} & v_{\mathrm{W}z}\\w_{\mathrm{W}x} & w_{\mathrm{W}y} & w_{\mathrm{W}z}\end{bmatrix}\begin{bmatrix}\cos\gamma\cos\chi\\\cos\gamma\sin\chi\\-\sin\gamma\end{bmatrix}V_\mathrm{K} \quad (6)$$

With small wind gradients and small χ and γ, equation (6) becomes

$$\begin{bmatrix}\dot{u}_\mathrm{W}\\\dot{v}_\mathrm{W}\\\dot{w}_\mathrm{W}\end{bmatrix} \approx \begin{bmatrix}u_{\mathrm{W}x}\\v_{\mathrm{W}x}\\w_{\mathrm{W}x}\end{bmatrix}V_\mathrm{K} \quad (7)$$

The resulting set of differential equations lends itself to be divided into two independent subsets, covering the "symmetrical" and "asymmetrical" state variables und thus dividing the model into separate descriptions of the longitudinal and lateral motion. For this analysis, we focus on the lateral part of the equations, because, due to the stronger restrictions on runway width compared to

runway length the lateral landing accuracy is of greater importance than the longitudinal landing accuracy here.

With $v_{\mathrm{W}} = \beta_{\mathrm{W}} V_{\mathrm{A}}$, $\beta_{\mathrm{K}} = \chi - \Psi$ and $\dot{\Psi} = r_{\mathrm{K}}$ (for small Φ), the simplified nonlinear differential equations for the lateral motion are:

$$\begin{bmatrix} \dot{\beta}_{\mathrm{W}} V_{\mathrm{A}} \\ \dot{r}_{\mathrm{K}} \\ \dot{\beta}_{\mathrm{K}} V_{\mathrm{K}} \\ \dot{p}_{\mathrm{K}} \\ \dot{\Phi} \\ \dot{\chi} V_{\mathrm{K}} \\ \Delta \dot{R}_y \end{bmatrix} = \begin{bmatrix} v_{\mathrm{W}x} V_{\mathrm{K}} \\ (I_{zx}/\Delta) L^{\mathrm{A}} + (I_x/\Delta) N^{\mathrm{A}} \\ (1/m) F_{\mathrm{Y}} + \sin\Phi \cos\Theta\, g - r_{\mathrm{K}} V_{\mathrm{K}} \\ (I_z/\Delta) L^{\mathrm{A}} + (I_{zx}/\Delta) N^{\mathrm{A}} \\ p_{\mathrm{K}} + \tan\Theta\, r_{\mathrm{K}} \\ (1/m) F_{\mathrm{Y}} + \sin\Phi \cos\Theta\, g \\ -\Delta\chi V_{\mathrm{K}} \end{bmatrix} \tag{8}$$

Summarized, the simplifications to yield equation (8) are:

- Small velocities p_{K}, q_{K}, r_{K}, v_{K} and w_{K}.
- Small angles α, β_{W}, β_{K}, $(\chi - \Psi)$ Θ, γ and Φ.
- Small wind values $u_{\mathrm{W}}/V_{\mathrm{A}}$, $v_{\mathrm{W}}/V_{\mathrm{A}}$, $w_{\mathrm{W}}/V_{\mathrm{A}}$ and wind gradients $u_{\mathrm{W}x}$, $u_{\mathrm{W}y}$, ...

In order to linearize equation (8), a reference state has to be chosen at which the nonlinearities are replaced by linear approximations (first order Taylor series) that are valid only in close vicinity of the reference state. Choosing symmetrical and trimmed forward flight at V_0 as a reference state and splitting the forces and moments into parts only dependent on a single state variable, the linearized equation of the lateral motion becomes:

$$\begin{bmatrix} \delta\dot{\beta}_{\mathrm{W}} \\ \delta\dot{r}_{\mathrm{K}} \\ \delta\dot{\beta}_{\mathrm{K}} \\ \delta\dot{p}_{\mathrm{K}} \\ \delta\dot{\Phi} \\ \delta\dot{\chi} \\ \delta\dot{D} \end{bmatrix} = \begin{bmatrix} 0 & 0 & 0 & 0 & 0 & 0 & 0 \\ -N_\beta & N_r & N_\beta & N_p & 0 & 0 & 0 \\ F_{Y_\beta} & -1 & F_{Y_\beta} & 0 & (g/V_0) & 0 & 0 \\ -L_\beta & L_r & L_\beta & L_p & 0 & 0 & 0 \\ 0 & \Theta_0 & 0 & 1 & 0 & 0 & 0 \\ -F_{Y_\beta} & 0 & F_{Y_\beta} & 0 & (g/V_0) & 0 & 0 \\ 0 & 0 & 0 & 0 & 0 & V_0 & 0 \end{bmatrix} \begin{bmatrix} \delta\beta_{\mathrm{W}} \\ \delta r_{\mathrm{K}} \\ \delta\beta_{\mathrm{K}} \\ \delta p_{\mathrm{K}} \\ \delta\Phi \\ \delta\chi \\ \delta D \end{bmatrix} + \begin{bmatrix} 0 & 0 & 1 & 0 \\ N_\xi & N_\varsigma & -N_r & -N_p \\ 0 & F_{Y_\varsigma} & 0 & 0 \\ L_\xi & L_\varsigma & -L_r & -L_p \\ 0 & 0 & 0 & 1 \\ 0 & F_{Y_\varsigma} & 0 & 0 \\ 0 & 0 & 0 & 0 \end{bmatrix} \begin{bmatrix} \delta\xi \\ \delta\varsigma \\ \delta v_{\mathrm{W}x} \\ \delta w_{\mathrm{W}y} \end{bmatrix} \tag{9}$$

Here, $x = \left[\delta\beta_{\mathrm{W}}\ \delta r_{\mathrm{K}}\ \delta\beta_{\mathrm{K}}\ \delta p_{\mathrm{K}}\ \delta\Phi\ \delta\chi\ \delta D\right]^T$ is the system's state vector, while the rudder and aileron deflections ($\delta\xi$, $\delta\varsigma$) and the wind gradients($\delta v_{\mathrm{W}x}$, $\delta w_{\mathrm{W}y}$) form the input vector to the system, all expressed as deviations δ from their reference value.

With $\delta D = \Delta R_y$ being the lateral deviation from the reference flight path (localizer), the value of δD at the moment of touchdown can be directly used as a measure of lateral landing accuracy.

To simplify notation, the denominator δ is omitted from here on, even though the state and input variables still denote deviations from the reference flight state.

Values for the coefficients in the linear state-space equation (9) are calculated from [11] for an Airbus A300 in landing configuration at V_0 = 77 m/s as summarized in Table 1.

Table 1: Elements of the state and input matrices in eq. (9) for an A300 in landing configuration at V_0 = 77m/s

N_β:	0.3684	L_β:	-1.3807	F_{Y_β}:	0.0970
N_p:	-0.2200	L_p:	-0.7735	F_{Y_ς}:	0.0225
N_r:	-0.2308	L_r:	0.7747	g/V_0:	0.1274
N_ξ:	-0.0245	L_ξ:	-0.2586		
N_ς:	-0.3551	L_ς:	0.0730	(SI units, angles in rad)	

2.2 Wind model

Turbulence is modeled by use of a white noise signal with a defined seed, filtered to create stochastic data with Dryden gusts' power spectral density. This approach allows easy generation of a great number of different reproducible and representative wind gradient time series for the monte-carlo simulations.

2.3 Sensor model

The technical implementation of a suitable atmospheric data sensor (e.g. LIDAR sensor) is not subject of this analysis. Instead we postulate the availability of such sensors in the near future. However, some physical limitations of these sensors are foreseeable and will be included into the analysis.

- A forward looking sensor mounted on the aircraft will have a limited sensor range.
- Sensors on the ground will most likely only measure data in a two-dimensional plane of

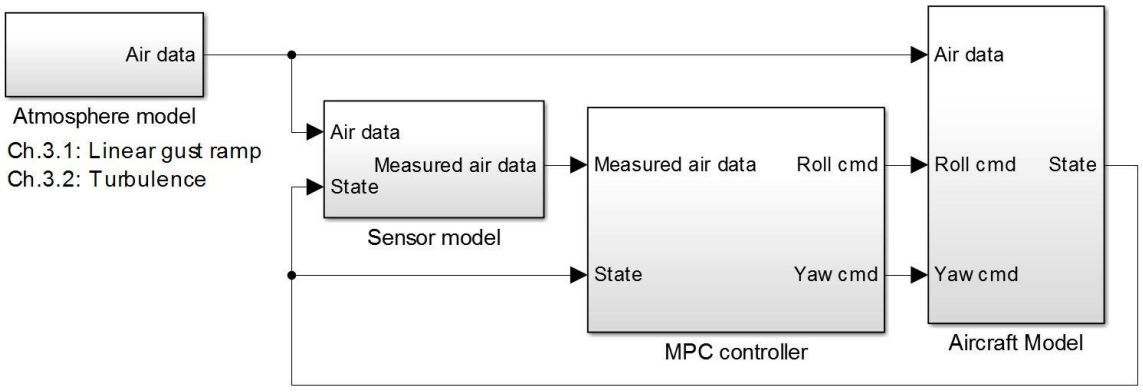

Fig. 4: Simulation structure

operation oriented perpendicular to the flight path of the aircraft and thus will give intermittent sets of data along the flight path.

Therefore, the simulation sensor model provides data with these limitations to the MPC algorithm.

3 Results

The outlined simulation model was used to design a model predictive controller that minimizes deviation from the reference flight path under the influence of atmospheric disturbances. A time step of 0.1 s and a prediction horizon of 10 s were chosen and the angles of the control surfaces (ξ, ς) were limited to ± 20°. In order to emphasize the minimization of the lateral deviation from the reference path, only the states D and χ were included into the cost function of the MPC optimizer. The simulations were performed in a simulation structure as shown in figure 4.

3.1 Linear gust ramp

Figure 4 and 5 show the reaction of the MPC controlled aircraft to a lateral gust from the left. The gust consists of a 1 s rectangular pulse of the wind derivative v_{Wx} starting at t = 10 s (Fig. 5) resulting in an increase of β_W up to 5° after one second (Fig. 4). At t = 12 s a similar 1 s pulse to the opposite direction occurs, reducing β_W to 0° again. The system's reaction is shown for three different controller configurations:

1. The continuous lines show the development of the state variables and inputs over time, when the controller does not use any information at all about the actual measured disturbance (md) v_{Wx} (**no md**). The controller can only react to the deviations of the state variables. The gust causes a maximum deviation from the reference path of $|D|_{max} \approx 1.25$ m (t ≈ 15 s) before the aircraft returns to the reference flight path.

2. The dotted lines (**md range 0 s**) show the state variables and inputs with the same controller but this time provided with information about the disturbance currently affecting the aircraft. This disturbance could be measured e.g. by wind vanes or pressure probes on board of the aircraft. The inherent knowledge of the aircraft's reaction to a disturbance due to the internal model allows for a better optimization of the commanded variables and thus leads to a smaller deviation from the reference flight path with $|D|_{max} \approx 0.56$ m (t ≈ 12 s).

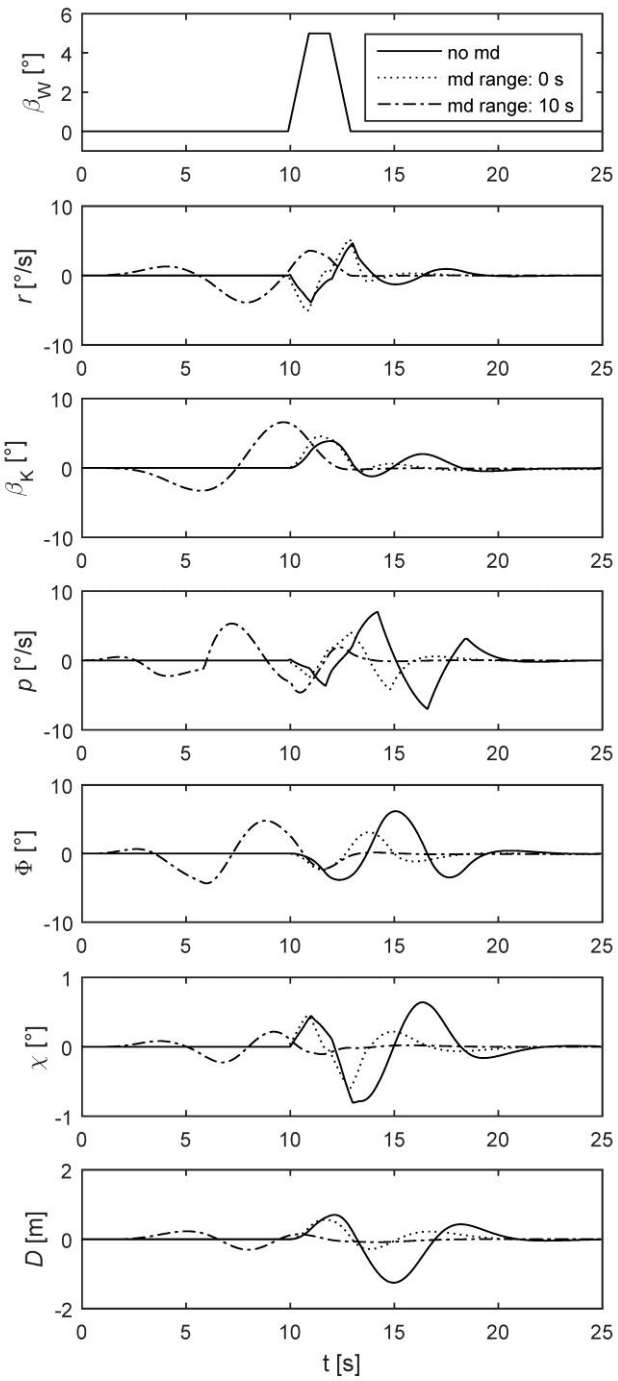

Fig. 4: States of the controlled system during gust, with and without measured disturbance (md)

3. The dash-dotted lines (**md range 10 s**) show the states of the system when the controller incorporates information about oncoming disturbances, measured up to 10 s ahead of the aircraft by LIDAR. With a landing speed of 77 m/s, the md range of 10 s gives an effective sensor range of 770 m. The maximum deviation from the reference flight path is further reduced to $|D|_{max} \approx 0.30$ m ($t \approx 8$ s).

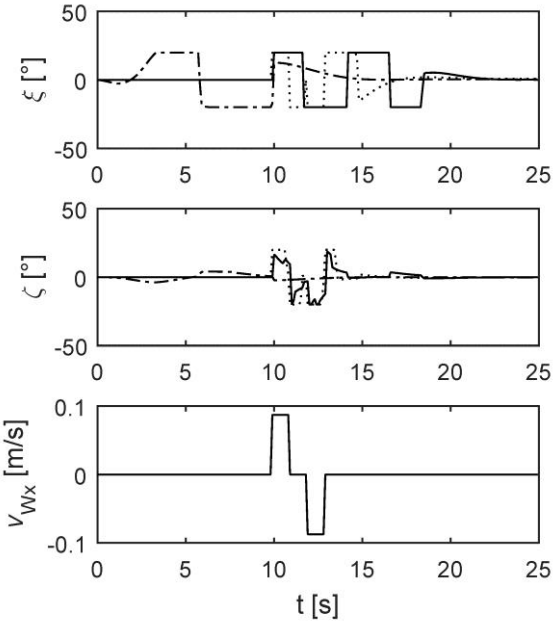

Fig. 5: Control surfaces and wind gradient during gust

The controller Configurations 1 and 2 are only able to react to the disturbance beginning from the moment the gust is actually affecting the aircraft. Consequently, counter steering with the control surfaces (ξ, ς) starts at t = 10 s (Fig. 5). Additionally, in this example, the gust declines before the system had time to settle at a new steady state, resulting in a significant overshoot when returning to the original trim state. Both, initial deviation and overshoot are less pronounced when the controller uses measured data of the currently affecting disturbance in order to predict the system's dynamic response to the disturbance more precisely (configuration 2).

In Configuration 3 however the controller does receive information about the oncoming disturbance beforehand und thus can prepare the system to better cope with the gust. Starting at $t \approx 2$ s, the controller, maneuvers the aircraft into a state that helps to reduce the effect of the oncoming gust, leading to a much smaller maximum deviation $|D|_{max}$ and a significantly reduced settling time. This is done at the price of small but acceptable deviations from the reference flight state prior to the gust.

In all three configurations, the controller is using full aileron control authority to counteract the atmospheric disturbance, leading to roll angles of more than 5°.

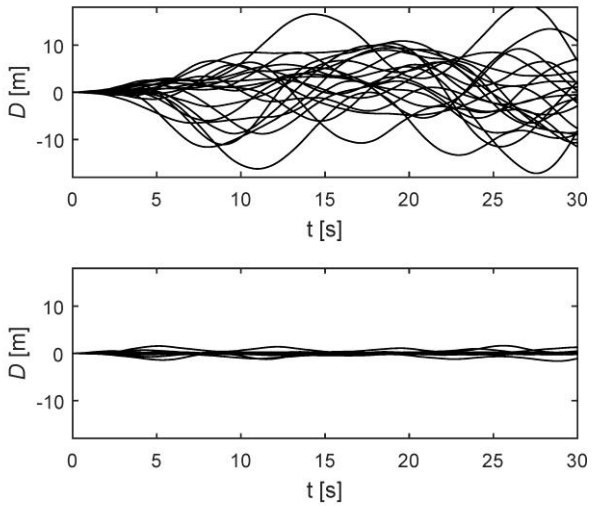

Fig. 6: 20 Monte-carlo simulations of the aircraft motion with MPC using md range of 0 s (top) and md range of 10 s (bottom)

3.2 Turbulence

Figure 6 shows a typical development of the lateral deviation D under turbulent atmospheric conditions for an aircraft with a controller using only currently measured disturbances at the aircraft (md range: 0 s) and a controller using measured disturbances for the full prediction horizon (md range: 10 s). For clarity only the first 20 monte-carlo simulations are displayed.

In both cases, the simulations start with the aircraft on the reference flight path. The turbulence induced lateral deviations are increasing quickly, resulting in maximum deviations of about 20 m in case of the controller using only current measurements. When using full measurement range however, the controller is able to keep the maximum deviations at a scale of 1 m.

The dependency between measurement range and standard deviation σ of the maximum deviations $|D|_{\max}$ is displayed in figure 7 for sets of 200 monte-carlo simulations. The standard deviation is decreasing from $\sigma \approx 4.3$ m to a value of $\sigma \approx 0.4$ m for a measurement range of 10 s (770 m) with the gradient flattening towards the prediction horizon. At a measurement range of 2 s (144 m) the deviation is reaching a local minimum of $\sigma \approx 0.8$ m.

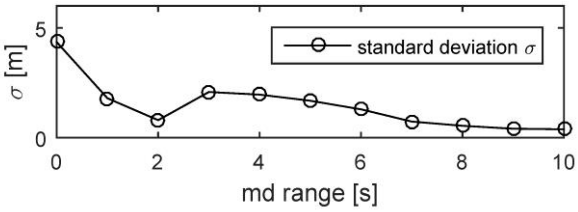

Fig. 7: Correlation between standard deviation of maximum deviations and range of measured disturbances (md)

3.3 Discussion of results

The simulations show that the deviations due to turbulence can be reduced by an order of magnitude when using the complete prediction horizon as sensor range. The results also show, that even with a measurement range of only 2 s, a significant reduction in deviations can be achieved. However, the temporary increase of the standard deviation when further increasing the measurement range beyond 2 s also shows, that the influence of the measurement range on the deviations is depending on additional factors. The results indicate that, while generally a long measurement range is preferable to reduce deviations, it is also possible to achieve good controller performance even with a very short measurement range, provided that e.g. the range fits to the system Eigen behavior and the characteristics of the turbulence. This will be subject of future analysis.

In the examined examples, the controller optimizes the complete flight path to stay close to the desired track and results are calculated with respect to the maximum deviation from the track. However, in a landing scenario the lateral deviation prior to touch-down is of less importance than the deviation at the moment of touch-down itself. Adapting the cost-function to reflect this by emphasizing the touch-down phase could further reduce deviation at that moment of contact with the runway.

Model Predictive Control allows a great number of parameters to be varied. This covers in particular the specification of the cost function with its weighting factors as well as the length of the prediction horizon or step size. These parameters have been chosen suitably for

the example control task, but have not been analyzed in depth. The use of full control surface authority (Fig. 4) for example is beneficial for fast turbulence compensation but could be less desirable in terms of passenger comfort or actuation effort of the control surfaces.

4 Conclusions and future work

This analysis aims to explore the general applicability of model predictive control in conjunction with atmospheric disturbance monitoring. The simulation results showed that the control approach is suitable to keep the aircraft on the desired flight track and that the control performance is further improved, if information about oncoming atmospheric disturbance is available.

While in general control performance improves with a longer range of the wind sensor, good results can already be achieved with a relatively short sensor range (Fig. 6). The good control performance in the regime of small sensor ranges is planned to be analyzed in more depth in future work.

The current analysis focused on the most relevant lateral motion of the aircraft. In a next step it is planned to extend the control scheme to the full aircraft motion. Performance analysis will then be carried out on a nonlinear 6DOF aircraft model.

References

[1] Barbaresco F. et al. Monitoring Wind, Turbulence and Aircraft Wake Vortices by High Resolution RADAR and LIDAR Remote Sensors in all Weather Conditions. *URSI Scientific Days*, 24-25th March, CNAM, Paris, 2015

[2] Yoshikawa E. and Matayoshi N., Wake Vortex Observation Campaign by Ultra Fast-Scanning LIDAR in Narita Airport, Japan. *Proc. 29th Congress of the International Council of the Aeronautical Sciences, St. Petersburg, Russia, 2014*

[3] Kameyama S., Yanagisawa T., Ando T., Sakimura T., Tanaka H., Furuta M. and Hirano Y. Development of wind sensing coherent Doppler LIDAR at Mitsubishi Electric Corporation –from late 1990s to 2013-. *Proc 17th Coherent Laser Radar Conference*, Barcelona, Spain, 2013.

[4] Matayoshi,N., Iijima T., Yoshikawa E., Ushio T. Development of Low-Level Turbulence Advisory System for Aircraft Operation. *Proc. 29th Congress of the International Council of the Aeronautical Sciences, St. Petersburg, Russia, 2014*

[5] Inokuchi H., Furuta M., and Inagaki T. High Altitude Turbulence Detection using an Airborne Doppler LIDAR. *Proc. 29th Congress of the International Council of the Aeronautical Sciences*, St. Petersburg, *Russia*, 2014

[6] Etkin B., Turbulent Wind and Its Effect on Flight, Journal of Aircraft, Vol. 1, No. 1, pp 327-34,1981

[7] Siepenkötter N., Pool D., Voskuijl M. et.al. Evaluation of Simulation Results. *GABRIEL GA No. FP7- 284884 , Deliverable 4.3.* 2014

[8] Rohacs D., Voskuijl M., Siepenkötter N., Evaluation of Landing Characteristics Achieved by Simulations and Flight Tests on a Small-Scaled Model Related to Magnetically Levitated Advanced Take-Off and Landing Operations. *Proc. 29th Congress of the International Council of the Aeronautical Sciences*, St. Petersburg, *Russia*, 2014

[9] MB+Partner: The future of flying? MB+Partner, http://www.mbptech.de/GroLaS_en.html 06/20/2016

[10] Camacho, E. F., Bordons Alba, C. *Model Predictive Control*, 2nd edition, Springer, 2008

[11] Brockhaus R., Alles W., Luckner R. *Flugregelung*, 3rd edition, Springer, 2011

Contact Author Email Address

mailto: siepenkoetter@fsd.rwth-aachen.de

Copyright Statement